Supporting Information: Influence of film thickness on Nafion interface structure, hydration and anisotropic ion transport

Steven C. DeCaluwe[1,2], Andrew M. Baker[2,3], Pavan Bhargava[2,4], John E. Fischer[1], Joseph A. Dura[2]

1. Department of Mechanical Engineering, Colorado School of Mines, Golden, CO, 80401, USA
2. NIST Center for Neutron Research, Gaithersburg, MD, 20899, USA
3. Department of Mechanical Engineering, University of Delaware, Newark, DE, 19716, USA
4. Department of Electrical Engineering and Computer Science, University of California, Berkeley, CA, 94720, USA

Details of Nafion thin film fabrication – All thin-film samples were prepared by spin-coating from a dispersion of Nafion* stock solution (1100 equivalent weight 20 wt% in solution of lower aliphatic alcohols and H_2O mixture; *Sigma Aldrich*) in HPLC grade ethanol (*Sigma Aldrich*). With a few exceptions, all films were spun for 60 seconds at 3500 RPM (58.3 Hz), and then heated for ≥ 1 hour at 60°C under vacuum to ensure solvent removal, adhesion to the substrate and consistent thermal history. For select samples with $t_{Naf} \geq 60$ nm, a two-stage spin-coating recipe was required to ensure a film free of defects and with suitable low surface roughness. Table S1 provides the spin-coat recipe (dispersion concentration, spin speeds, and time of spin speed) for all samples.

Table S1. Nafion-Ethanol dilutions and spin-coat recipes for all samples in the study.

Sample t_{Naf} (nm)	% volume Nafion dispersion in dilution	Stage 1 spin speed (RPM or Hz × 60)	Stage 1 time (s)	Stage 2 spin speed (RPM or Hz × 60)	Stage 2 time (s)
5	0.55	3500	60		
7	0.72	3500	60		
12	1.74	3500	60		
18	2.70	3500	60		
20	1.50	3500	60		
42	5.01	3500	60		
60	7.52	500	3	3500	60
103	11.11	550	4	3500	60
120	11.11	550	4	2000	60
153	7.52	500	10	3500	60

Neutron Reflectometry (NR) Fitting Summary Details – Table S2, below, provides details on the SLD profiles fitted to the NR data for each sample, including equivalent Nafion* thickness t_{Naf}, reduced χ^2 value, and the water volume fraction V_{water} for (*i*) the sheet-like lamellar region at the Nafion/SiO_2 interface, (*ii*) the lamellae-free bulk-like layer that forms between the lamellae and the vapor interface for films with $t_{Naf} \geq 12$ nm, and (*iii*) the sample as a whole.

Table S2. Equivalent Nafion thickness t_{Naf}, reduced χ^2 values, and average water volume fractions for the lamellae ($V_{water,lamellae}$), well-mixed bulk-like layer ($V_{water,bulk\text{-}like}$), and for the sample as a whole ($V_{water,average}$) for each sample. Numbers in brackets represent 68% confidence intervals.

Sample Name	**t_{Naf} (nm)**	**Reduced χ^2**	**$V_{water,lamellae}$ (%)**	**$V_{water,bulk\text{-}like}$ (%)**	**$V_{water,average}$ (%)**
t5	4.6 [4.6, 4.7]	1.06	21.4 [20.6, 21.6]	--	21.4 [20.6, 21.6]
t7	6.8 [6.8, 6.9]	0.90	23.5 [23.0, 23.6]	--	23.5 [23.0, 23.6]
t12	11.6 [11.5, 11.6]	1.26	16.7 [16.4, 16.9]	12.2 [12.3, 12.9]	15.2 [15.1, 15.5]
t18	17.8 [17.8, 17.8]	1.12	18.4 [18.2, 18.7]	15.2 [15.0, 15.3]	16.5 [16.5, 16.7]
t20	19.5 [19.5, 19.6]	1.17	18.1 [18.0, 18.3]	14.7 [14.6, 14.8]	16.0 [16.0, 16.1]
t42	41.9 [41.8, 41.9]	1.26	20.1 [20.0, 20.3]	17.6 [17.5, 17.7]	18.1 [18.0, 18.1]
t60	59.9 [59.7, 60.0]	0.81	32.5 [31.1, 32.0]	24.6 [24.4, 24.6]	25.5 [25.2, 25.4]
t103	102.8 [102.8, 102.9]	1.04	40.7 [40.6, 40.9]	24.6 [24.6, 24.7]	25.4 [25.4, 25.5]
t120	119.6 [119.7, 119.8]	0.92	37.4 [37.2, 37.6]	25.8 [25.7, 25.8]	26.3 [26.2, 26.2]
t154	154.0 [153.9, 154.2]	1.07	36.8 [36.3, 36.8]	25.5 [25.5, 25.5]	25.9 [25.9, 26.0]

Surface layers in the thick-film regime – For samples t103 and t120, suitable fits were obtained only when an additional layer was added to the SLD profile, at the Nafion/vapor interface. Reduced χ^2 values were ≥ 1.5 without these layers and < 1.2 with the layers, and adding the surface layer reduces the Bayesian Information Criterion (BIC) by 94 for t103 and by 182 for t120 (ΔBIC ≥ 12 is considered a "very strong" case for one model over another).[1] While the surface layers in Figure 3 have an SLD higher than that of the bulk-like layer, fits identified an additional suitable model, with the surface layer SLD < 0.0 nm^{-2}.

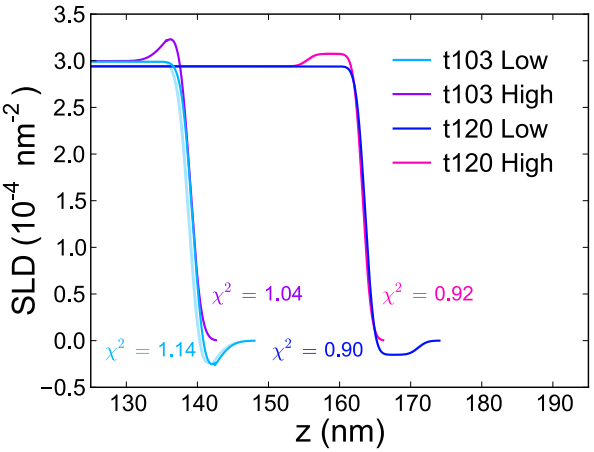

Figure S1. SLD profiles of surface layers required to fit NR data for samples t103 and t120, including reduced χ^2 values for each. The labels "Low" and "High" refer to the SLD of the surface layer, relative to the adjacent bulk-like layer. Solid lines show best fits, and shaded regions show 68% confidence intervals.

Figure S1 shows SLD profiles for all suitable surface layer fits. For both samples, models provide equally good fits (as shown by the χ^2 values), and result in equivalent t_{Naf} values. As such, neither model is preferred based upon the NR data alone. For the other samples with t_{Naf} ≥ 60 nm, suitable fits were obtained without any surface layers (χ^2 values of 0.81 and 1.07 for t60 and t153, respectively). It is not clear whether the surface layers were not present, perhaps due to slower spin-cast speed for these samples or other differences in sample history, or whether the data was simply not sensitive enough to require these surface layers (note that the Figure 2 data for these two samples have a significant number of data points with larger error than the other samples, due to experimental constraints). NR for sample t103 was also measured at 0% RH, and fits to this data were not improved by adding such a layer.

While the NR fits can not discriminate between these models on the basis of χ^2 values, physical interpretation of the fitted surface layer SLDs would suggest that the higher SLD surface layer is perhaps more likely. For the low-SLD surface layers, the most plausible physical interpretation is that these 3-5nm thick layers consist of adsorbed water (SLD_{H2O} = -5.6x10^{-5} nm^{-2}) mixed with a small amount of polymer material. While

we cannot rule them out entirely, such layers have not been observed previously for thin-film Nafion, and it is difficult to envision a mechanism by which such layers would form and maintain uniform thickness on the vertically oriented samples in this study. The high-SLD surface layer, meanwhile, would most likely correspond to the Fluorine-rich 'hydrophobic skin' hypothesized at the interface between humidified Nafion and vapor environments.[2–6] In our previous paper, the SLD of the fluorocarbon backbone was estimated at 4.776×10^{-6} nm^{-2} – slightly higher than that of dry, well mixed Nafion 1100 ($SLD_{\text{Nafion}} = 4.16 \times 10^{-6}$ nm^{-2}). A slightly fluorine-rich Nafion morphology with an SLD slightly higher than that of adjacent the bulk-like Nafion layer, as proposed by the profiles for 't103 High' and 't120 High' in Figure S1, is therefore consistent with the previously observed fluourine-rich layers. Follow-up NR studies with contrast variation (e.g., humidified with H_2O and then with D_2O) could possibly determine the SLD of these surface layers, to determine if these layers can be observed for a range of thicknesses > 60 nm, or alternately if their formation is somehow dependent on the sample fabrication and measurement history.

Average lamellar water content as a function of distance from the substrate – To better understand the relationship between the lamellar and bulk-like layer water uptake, we calculate here a "moving average" of the water content in the lamellae. Because we have shown that the Nafion moieties phase-segregate between the layers in the lamellae,[1] the Nafion stoichiometry (1100 EW) is only preserved when averaging over multiple layers. The side-chains and backbone molecules corresponding to the sulfonic acid groups in a given water-rich layer are located in the layer itself, plus its two nearest-neighbors. In addition, it is necessary to average over the water rich and water poor lamellae to suitably compare the water content to that of the mixed domain bulk-like layer. As such, the relevant way to compare V_{water} between the lamellae and bulk is to look at the moving average of $V_{\text{water,lamellae}}$ – the water content of a given layer, plus its two nearest neighbors, with V_{water} for each layer weighted by its thickness.

For the layers adjacent to the SiO_2 and to the bulk-like layer, this is the average of the layer plus its nearest neighbor:

$$V_{\text{water,avg}}(j) = \frac{V_{\text{water}}(j)\, t(j) + V_{\text{water}}(j+1)\, t(j+1)}{t(j) + t(j+1)}, \qquad j = 1. \quad \text{(S1)}$$

$$V_{\mathrm{water,avg}}(j) = \frac{V_{\mathrm{water}}(j-1)\, t(j-1) + V_{\mathrm{water}}(j)\, t(j)}{t(j-1)+t(j)}, \qquad j = n_{\mathrm{layers}}. \quad \text{(S2)}$$

For all other layers, it is the average of the layer plus its two nearest neighbors:

$$V_{\mathrm{water,avg}}(j) = \frac{0.5\, V_{\mathrm{water}}(j-1)\, t(j-1) + V_{\mathrm{water}}(j)\, t(j) + 0.5\, V_{\mathrm{water}}(j+1)\, t(j+1)}{0.5\, t(j-1) + t(j) + 0.5\, t(j+1)}, \; 1 < j < n_{\mathrm{layers}}. \quad \text{(S3)}$$

The results are shown in Figure 5 and discussed in detail in the main body of the manuscript, for the thin-film (Figure 5(a)) and thick-film (Figure 5(b)) regimes. Additionally, for the thick-film samples with a surface layer (t103 and t120), $V_{\mathrm{water,avg}}$ is significantly higher in layers 3 and 4 than for those with no surface layer. Given the limited number of samples investigated and the differences in fabrication history discussed above, with regard to the surface layer phenomenon, it is unclear if these differences are real, are a somehow a fitting artifact related to the effects of the surface layer on the NR fits, or are otherwise related to differences in sample fabrication or sample-to-sample variation. For these reasons we refrain from commenting further on these differences in the $V_{\mathrm{water,avg}}$ profile, but simply comment that they merit additional study.

Predicted conductivities using bulk Nafion relationships – predicted sample conductivities $\sigma_{\mathrm{parallel}}$, σ_{normal}, and $\sigma_{\mathrm{average}}$ using standard relationships for bulk Nafion 1100 (Eqs. 2, 4 and 5) are shown in Figure S2. For all films, the predicted conductivities are higher than those measured at similar thicknesses by Paul, et al,[9] thus motivating the conductivity scaling models discussed in the main text and below. $\sigma_{\mathrm{average}}$ is the conductivity predicted if $V_{\mathrm{water,average}}$ (e.g. *via* a technique that is insensitive to composition depth profile) were used to calculate the conductivity *via* eqs. 4 and 5. The dashed line represents the conductivity of bulk Nafion at this T and RH value.[7,8] These predictions show two noteworthy trends, with increasing thickness: (*i*) for the thinnest films (t7 through t20) the conductivity values decrease upon formation of the thin, relatively dry bulk-like layer (at t12), and then increase as the water content of the bulk-like layer increases with increasing film thickness; (*ii*) the conductivity anisotropy decreases (i.e. $\sigma_{\mathrm{parallel}}$ and σ_{normal} become more similar) with increasing thickness, due to the increasing contribution from the well mixed, isotropic bulk-like layer. There is an interesting increase in anisotropy for sample t60, due to the significant increase in the

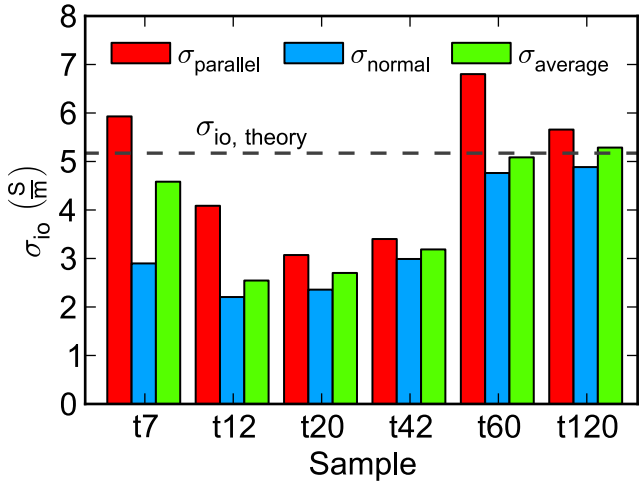

Figure S2. Predicted effective ion conductivities using standard (bulk) Nafion relationships (Eqs. 2, 4, and 5). Conductivities are higher than measured values for all samples.[9] '$\sigma_{parallel}$' and 'σ_{normal}' correspond to transport direction, relative to the substrate plane, as in Figure 1. 'σ_{averge}' is based on the average water content of the film as a whole, ignoring polymer ionic domain structure variations in the through-plane direction. Dashed line shows the conductivity of bulk Nafion at 29.6 °C and 92% RH.

lamellar water content between samples t42 and t60, as shown in Figure 5; this anisotropy mostly disappears for sample t120, as the thick bulk-like layer dominates the conductivity. We also see that, for samples with no bulk-like layer, knowing the concentration depth profile is essential to correctly predict the conductivity: the conductivity calculated using the average water content ($\sigma_{average}$) is significantly different from both $\sigma_{parallel}$ and σ_{normal}.

Alternative conductivity scaling models – In addition to Models 1–4 presented in the main body of the manuscript, alternative models to scale the individual layer conductivities were proposed and tested, and are presented here for the sake of completeness:

- Model 5 (2 parameters): The ionic conductivity of the water-rich layer adjacent to the SiO_2 is scaled by $C_{interface}$, and the conductivities for all other layers are multiplied by C_{film}.
- Model 6 (3 parameters): The ionic conductivity of the water-rich layer adjacent to the SiO_2 is scaled by $C_{interface}$, the conductivities of all other lamellae are scaled by $C_{lamellae}$, and the conductivity of the bulk-like layer (and surface layer, if present) is multiplied by $C_{bulk\text{-}like}$.

These two models test the hypothesis that the ion mobility in the water-rich layer adjacent to the SiO_2 substrate is fundamentally different from that in all other layers, due to the bonding of the terminal SO_3H groups to the substrate and high λ value ($\lambda > 22$). As shown by the results in Figure S3, neither model fits the data particularly well, with sum of squared residual (SSR) values that are significantly higher than for Models 3 and 4 in the main body of the manuscript (SSR = 0.651 for Model 5, SSR = 0.008 for Model 6). While the SSR for Model 6 is low, it is larger than that for Model 4 (SSR = 0.001), which has the same number of parameters. As with Model 2, Model 6 incorrectly predicts increasing conductivity with decreasing thickness in the thin-film and truncated regimes. Rather than a separate scaling factor for the layer at the SiO_2 interface, these fits reinforce the conclusion that there is a gradient in the ion mobility,

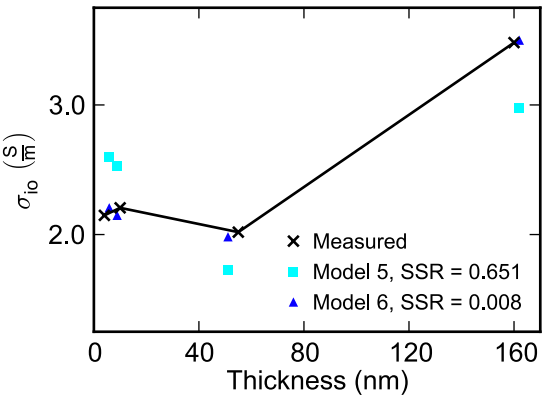

Figure S3. Measured (×) and predicted (filled symbols) lateral conductivities for Nafion thin films at 30°C with varying thickness. Predicted σ_{io} values come from NR composition profiles, using Eqs. 8, 9, and 11 for individual layer conductivities, which are scaled according to one of two models. Each model hypothesizes how confinement and the lamellar morphology affect ionic conductivity, as described in the text. SSR for each model represents the sum of squared residuals. Experimental data from Paul, *et al.*[9] Lines are drawn to connect experimental data points for ease of visualization.

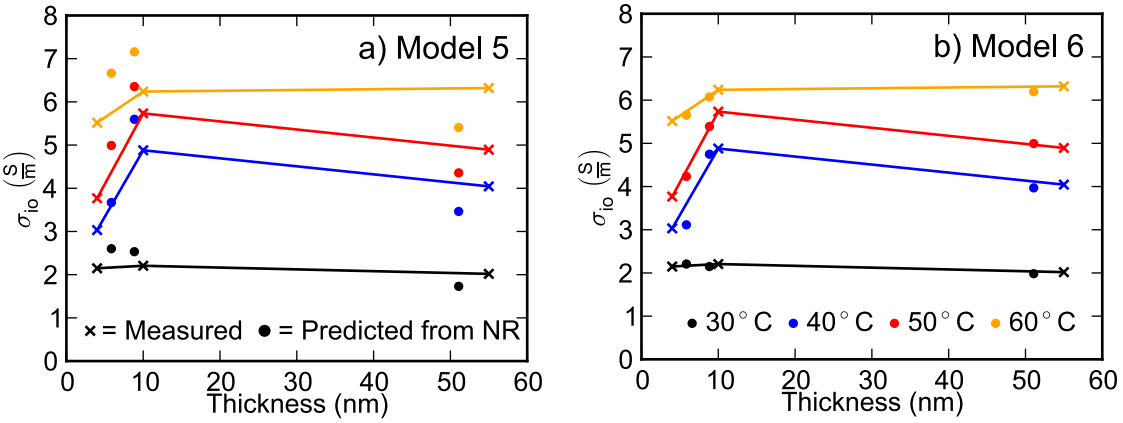

Figure S4. In-plane ionic conductivity as a function of temperature and film thickness, for the two conductivity models fitted to the experimental data in Figure S3. × = Experimental data from Paul, *et al.*[9] with lines drawn to connect the data points for ease of visualization. • = Prediction from NR. Results show that the insights from models 3 and 4, in which the ion mobility varies throughout the film thickness (both bulk-like layer vs. lamellae, and within the lamellae) are required to predict and explain conductivity trends with varying thickness at relevant operating temperatures.

which increases with increasing distance from the substrate. Figure S4 shows the variation in the predicted conductivity at elevated temperatures for Models 5 and 6, which follow expected trends, based on the results in Figure S3 and in the main manuscript. Model 5 gives a poor match to the measured data at all thicknesses and all temperatures. Model 6 provides a suitable fit, but appears slightly worse than Model 4, in the main manuscript.

Activation energies for thin-film Nafion conductivity values – The dependence of the ionic conductivity on temperature variations was modeled as a thermally-activated process with an Arrhenius-type dependence:

$$\sigma_{io} = \sigma^{\circ} \exp\left(-\frac{E_a}{RT}\right), \qquad \text{(S4)}$$

where σ° is the pre-exponential factor, E_a the activation energy, R the universal gas constant, and T the sample temperature. Activation energies were fit to the data presented in the supporting information of the publication by Paul, *et al.*[9] by fitting the plot of $-\ln(\sigma_{io})$ vs.

Table S2. Fitted Arrhenius parameters for Nafion thin film conductivity σ^{o} (10^3 S/m) and E_a (kJ/mol-K), as plotted in Figure S5.

t_{film}	$T \leq 40^{o}C$		$40^{o}C \leq T \leq 60^{o}C$	
	σ^{o}	E_a	σ^{o}	E_a
4	104.2	27.18	61.0	25.86
10	$1.3*10^8$	62.60	0.3	10.68
55	$5.6*10^6$	54.79	6.7	19.31

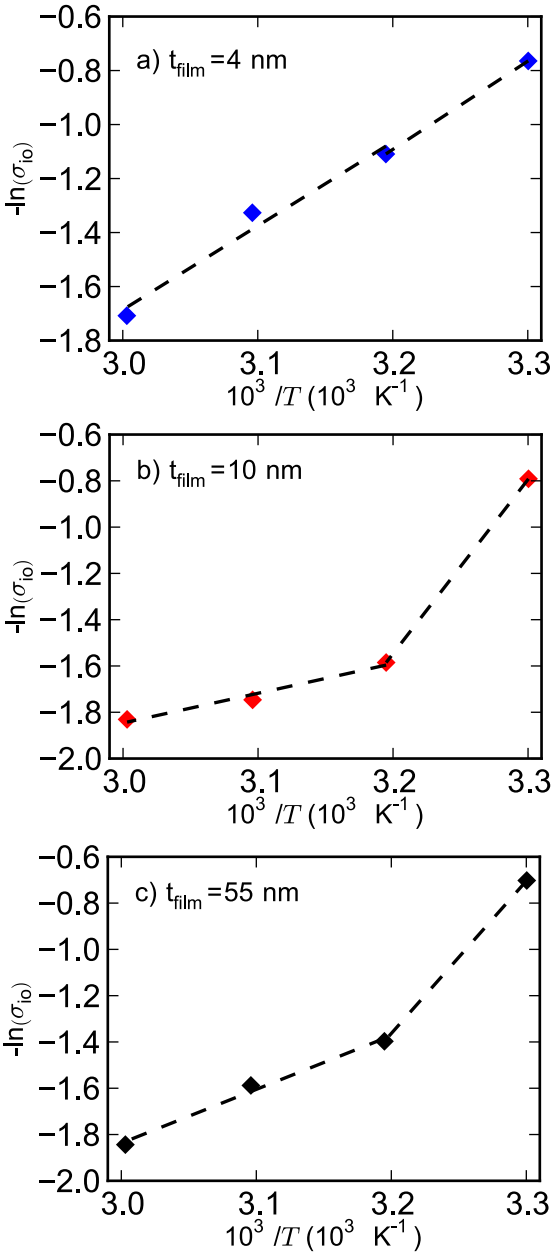

Figure S5. Conductivity as a function of temperature for films of thickness: a) t_{film} = 4 nm, b) t_{film} = 10 nm, and c) t_{film} = 55 nm. Reproduced from Paul, *et al.*[9] with permission of the author. Data is fit to an Arrhenius-type (dashed lines) to calculate activation energies for $T \leq 40^{o}C$ and $40^{o}C \leq T \leq 60^{o}C$.

$1/T$ to a linear equation. In this manner, the slope is interpreted as E_a/R and the intercept as $-\ln(\sigma^\circ)$. Plotting the temperature variations for 4 nm $\leq t_{film} \leq$ 160 nm, (Figure S5) two separate activation energies are identified for the three samples with $t_{film} > 4$ nm: one for $30^oC \leq T \leq 40^oC$, and one for $40^oC \leq T \leq 60^oC$. To be consistent, the same approach was applied for $t_{film} = 4$ nm, as well. The fits are shown as the dashed lines in Figure S5. The fitted parameters σ° and E_a for the low-temperature ($T \leq 40^oC$) and high-temperature ($40^oC \leq T \leq 60^oC$) regimes are provided in Table S2.

References Cited.(1) DeCaluwe, S. C.; Kienzle, P. A.; Bhargava, P.; Baker, A. M.; Dura, J. A. *Soft Matter* **2014**, *10* (31), 5763.

(2) Bass, M.; Berman, A.; Singh, A.; Konovalov, O.; Freger, V. *J. Phys. Chem. B* **2010**, *114* (11), 3784.

(3) Daly, K. B.; Benziger, J. B.; Panagiotopoulos, A. Z.; Debenedetti, P. G. *J. Phys. Chem. B* **2014**, *118* (29), 8798.

(4) Dowd, R. P.; Day, C. S.; Van Nguyen, T. *J. Electrochem. Soc.* **2017**, *164* (2), F138.

(5) Kongkanand, A. *J. Phys. Chem. C* **2011**, *115* (22), 11318.

(6) Majsztrik, P. W.; Satterfield, M. B.; Bocarsly, A. B.; Benziger, J. B. *J. Memb. Sci.* **2007**, *301* (1–2), 93.

(7) Zawodzinski Jr, T.; Springer, T.; Uribe, F.; Gottesfeld, S. *Solid State Ionics* **1993**, *60* (1–3), 199.

(8) Springer, T. E.; Zawodzinski, T. A.; Gottesfeld, S. *J. Electrochem. Soc.* **1991**, *138* (8), 2334.

(9) Paul, D. K.; Mccreery, R.; Karan, K. *J. Electrochem. Soc.* **2014**, *161* (14), 1395.

* Certain commercial equipment, instruments, materials, suppliers, or software are identified in this paper to foster understanding. Such identification does not imply recommendation or endorsement by the National Institute of Standards and Technology, nor does it imply that the materials or equipment identified are necessarily the best available for the purpose.